ELSEVIER

Advances in Water Resources 24 (2001) 1069–1083

Advances in Water Resources

www.elsevier.com/locate/advwatres

A re-examination of modeled and measured soil moisture spatial variability and its implications for land surface modeling

C.D. Peters-Lidard [a,*], F. Pan [a], E.F. Wood [b]

[a] *School of Civil and Environmental Engineering, Georgia Institute of Technology, Atlanta, GA 30332-0355, USA*
[b] *Department of Civil and Environmental Engineering, Princeton University, Princeton, NJ 08544, USA*

Received 3 July 2000; received in revised form 14 March 2001; accepted 10 April 2001

Abstract

Using a spatially distributed water and energy balance model, we investigate the spatial structure of surface fluxes and states for the Washita '92 field experiment and the August campaign of the Washita '94 field experiments. For Washita '92, the model is validated against gravimetric and remotely sensed soil moisture, and for Washita '94, the model is validated against gravimetric soil moisture and measured energy fluxes. The model is shown to reasonably represent land–atmosphere interactions during the experimental periods. Scaling analysis of remotely sensed and modeled soil moisture and modeled latent heat flux is indicative of multiscaling behavior. The temporal behavior of the soil moisture scaling exponents for various moments suggests the existence of three distinct regimes during a dry-down. The multiscaling behavior inferred from simulated soil moisture and latent heat flux is hypothesized as a relationship which is a function of average soil moisture. Similar scaling analysis of important land surface properties indicates simple scaling for porosity, field capacity and wilting point, and multiscaling for residual soil moisture, leaf area index and the soils-topographic index. This is consistent with model results, which indicate a transition from simple scaling to multiscaling with dry-down. It is hypothesized that this transition is governed by the scaling properties which in wet conditions control infiltration (porosity, field capacity, leaf area index) to properties which in dry conditions control drainage (residual moisture content and soils-topographic index) and evaporation (wilting point, leaf area index). Land surface models which fail to incorporate these features will most likely be unable to capture the dynamic nature of soil moisture spatial variability. © 2001 Published by Elsevier Science Ltd.

1. Introduction

There has been considerable interest of late in the scaling properties of soil moisture, given its importance in land–atmosphere interaction, as well as agricultural, hydrologic and ecological applications. This endeavor has been given a sense of urgency as scientists seek to employ the forthcoming satellite-based soil moisture products in models and analyses which seemingly require more spatial detail.

One of the earliest works to suggest that remotely sensed soil moisture is a multiscaling field was that of Rodriguez-Iturbe et al. [23], who analyzed the Washita '92 [11,12] 200 m resolution airborne ESTAR L-band soil moisture products from June 11, 14 and 18. In addition, they, along with Wood [27] and Burrough [3], studied the scaling properties of porosity in order to investigate the logical causal link between the scaling properties of porosity and soil moisture. Later analyses with the same data have provided strong evidence for multiscaling which changes with moisture condition [4,9]. Dubayah et al. [4] applied a spatially distributed water and energy balance model and found that the model did not reproduce the moisture-dependent scaling behavior of the ESTAR soil moisture fields. Hu et al. [9] provide sound empirical evidence for the multiscaling behavior, and decompose the fields to identify simple scaling behavior for the small-scale components. In addition, they question the results of Wood [27], in which scaling analysis of the model-derived soil moisture fields for the same period show an upward concavity which increases with dry-down. This counter-intuitive behavior seems to have been partially corrected by Dubayah et al. [4], who apply essentially the same model to the same period with the modifications of a thin soil layer and soil resistance parameterization as described by Peters-Lidard et al. [19].

* Corresponding author. Tel.: +1-404-894-5190; fax: +1-404-385-1131.
E-mail address: cpeters@ce.gatech.edu (C.D. Peters-Lidard).

0309-1708/01/$ - see front matter © 2001 Published by Elsevier Science Ltd.
PII: S0309-1708(01)00035-5

As Wood [30] notes, the progress in scaling of hydrologic remote sensing and scaling of hydrologic processes at the 10^3 km^2 scale has been minor due to lack of reliable datasets as well as deficiencies in field experiment design. Quantifying the spatial structure of surface fluxes and states is critical for comparisons with and

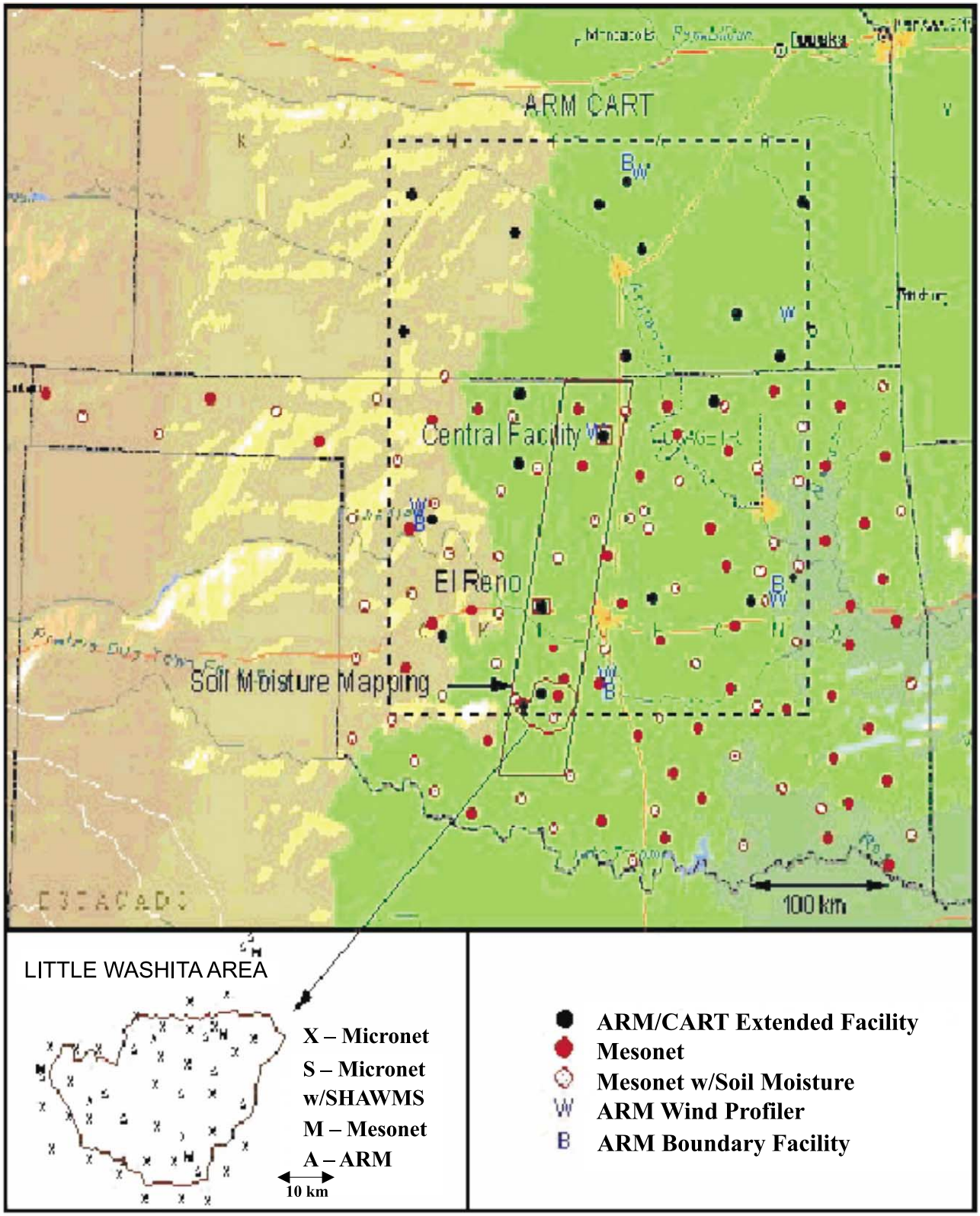

Fig. 1. Southern Great Plains Hydrology Experiment area, showing the location of the Little Washita Watershed, OK.

incorporation of remotely sensed measures of these quantities in land–atmosphere models. In addition, it may be important for "subgrid" turbulence parameterizations in numerical weather prediction and climate models to represent the buoyant production of turbulent kinetic energy due to latent and sensible heat flux variability. Thus, if simple relations between small- and large-scale statistics of soil moisture and/or surface latent and sensible heat fluxes can be found, small-scale variability in the flux might be inferred from a coarser resolution model.

In this work, we employ a spatially distributed water and energy balance model to investigate the spatial structure and scaling properties of surface soil moisture as well as the surface latent heat flux. Our analysis of modeled fluxes and states is presented in three sections. Section 2 presents the application of a spatially distributed water and energy balance model to the Little Washita Watershed (Fig. 1) for the June 12–18 Washita '92 [11,12] and August '94 field campaign [25], including validating the model output as well as assessing the spatial variability of model fluxes and states with time. An assessment of the scaling behavior of the model output soil moisture and latent heat flux is given in Section 3, and Section 4 focuses on physical interpretation of these results in the context of land surface modeling.

2. Model application and validation

Simulation of the water and energy balance of the approximately 530 km^2 Little Washita Watershed is carried out via the explicitly distributed TOPMODEL-based land–atmosphere transfer scheme (TOPLATS-GIS) as described in [18,19]. This model is based on the previous work of several authors [1,5,6,16,24,28,29,31], and differs from that employed in [4,27] because all land surface properties are "explicitly" distributed rather than "statistically" distributed according to the TOPMODEL topographic index. This capability allows for the explicit representation of potentially important local controls such as soil texture and land cover, which may become more important than the non-local topographic control during a dry-down as discussed by Western et al. [26] and Grayson et al. [7]. TOPLATS-GIS simulates vertical heat and moisture diffusion through the unsaturated zone for each computational element, while approximating redistribution of water in the saturated zone according to TOPMODEL.

2.1. Parameter estimation

The TOPLATS model was configured to facilitate comparisons with gravimetric soil moisture data and ESTAR L-band soil moisture products, both of which represent the upper 5 cm of soil. The geometric parameters are shown in Table 1. Three other categories of parameters are required: TOPMODEL, soils and land cover. TOPMODEL parameters are constant for a given watershed, while the soils and land cover parameters vary spatially according to soil and land cover type. TOPMODEL parameters were estimated based on a base flow recession analysis using historical stream flow data, and are given in Table 1 along with other spatially constant parameters, which were estimated a priori following [18,19,21] for the soil parameters and [2,13,20] for the land cover parameters. Spatially variable soil and land cover parameters are given in Tables 2 and 3, respectively. The parameters in Tables 2 and 3 were mapped to 30 m soil texture and land cover images for the watershed. A detailed description of the soil texture and land cover images, as well as a statistical and spatial analysis of important topographic, soil and land cover parameters and near-surface micrometeorological data, is contained in [17]. In addition to the parameters in Tables 1–3, the soils-topographic index [17,24] is derived from 30 m DEM data as input to the model.

2.2. Forcing and validation data

The data used in this work both for verification and model forcings were collected and/or compiled during the June Washita '92 [11] and August campaign of Washita '94 [25]. For Washita '92, model forcing data are derived from four temporary meteorological stations

Table 1
Spatially constant parameters for the Little Washita

Parameter	Symbol	Value
Geometry		
Thermodynamic data height (m)	z_a	1.5
Wind data height (m)	z_w	2.0
Layer 1 soil temperature depth (m)	z_1	0.05
Layer 2 soil temperature depth (m)	z_2	0.50
Surface zone moisture store depth (m)	z_{sz}	0.05
TOPMODEL parameters		
Average soils-topographic index	λ	8.70
Hydraulic conductivity decay parameter (m^{-1})	f	5.0
Base flow at saturation (m^3/s)	Q_0	83.48
Area (km^2)	A	530
Soil parameters		
Soil resistance parameter 1 (s/m)	r_{min}	3.8113×10^4
Soil resistance parameter 2	C_s	−13.515
Vegetation parameters		
Minimum stomatal resistance (s/m)	r_{stmin}	75.00
F(PAR) parameter 1 (s/m)	r_{stmax}	5000
F(PAR) parameter 2 (W m^{-2})	R_{pl}	100
$F(q)$ parameter 1	β	0.0002
$F(T)$ parameter 1 (K^{-2})	$B1$	0.00016
Field capacity	θ_{cap}	0.325
Wilting soil moisture	θ_w	0.07

Table 2
Little Washita soil texture occurrence and model parameters

Soil texture	% Area	Pore size index	Bubb. press. (m)	Porosity	Resid. sat.	Field capacity	Sat. hyd. cond. (m/s)	Wilting point	Dry soil heat cap. (K m/s)	Quartz cont.
Silt loam	32.59	0.234	0.208	0.501	0.015	0.282	1.889e − 6	0.133	1.27e + 6	0.25
Sandy loam	28.81	0.378	0.302	0.453	0.041	0.230	7.194e − 6	0.095	1.34e + 6	0.60
Clay loam	0.06	0.242	0.564	0.464	0.075	0.365	6.389e − 7	0.197	1.23e + 6	0.35
Loam	10.14	0.252	0.401	0.463	0.027	0.281	3.660e − 6	0.117	1.21e + 6	0.40
Sand	9.62	0.694	0.160	0.437	0.020	0.155	5.833e − 5	0.033	1.47e + 6	0.92
Loamy sand	18.61	0.553	0.206	0.437	0.035	0.180	1.697e − 5	0.055	1.41e + 6	0.82
Silty clay loam	0.17	0.177	0.703	0.471	0.040	0.337	4.167e − 7	0.208	1.32e + 6	0.10

Table 3
Little Washita land cover type occurrence and model parameters

Cover type	% Area	LAI	Albedo (dry)	Albedo (wet)	Emiss.	$z_{0,m}$	$z_{0,h}$	d_0
Water	0.30	0.00	0.15	0.15	0.98	0.005	0.0005	0.00
Summer crops	7.16	1.50	0.20	0.24	0.95	0.05	0.005	0.10
Bare soil	6.09	0.00	0.20	0.15	0.95	0.01	0.001	0.01
Natural pasture	33.31	2.00	0.20	0.24	0.95	0.05	0.005	0.10
Alfalfa/oats	14.98	1.50	0.20	0.24	0.95	0.05	0.005	0.10
Rangeland/trees	38.15	3.00	0.20	0.24	0.95	0.10	0.010	0.50

as discussed by Kustas et al. [14]. These data include solar radiation, air temperature and humidity and wind speed. For Washita '94, model forcing data include 1.5 m air temperature and humidity, downward solar radiation and precipitation from 42 USDA/ARS Micronet stations (with an average inter-station spacing of about 5 km) and 2 m wind speed and pressure from four nearby Oklahoma Mesonet stations. For both experiments, downward longwave radiation was not available and was estimated using station data following a variation of the Stefan–Boltzmann law as given in [2]:

$$R_{\mathrm{ld}} = E_{\mathrm{a}}\sigma T_{\mathrm{a}}^4, \tag{1}$$

where σ is the Stefan–Boltzmann constant, T_{a} is the air temperature in Kelvin, and E_{a} is the emissivity of the atmosphere:

$$E_{\mathrm{a}} = 1 - 0.261\exp[-7.77\times10^{-4}(273 - T_{\mathrm{a}})^2]. \tag{2}$$

The model was run for both experimental periods at a 30 m resolution with an hourly time step. All input "forcing" data were interpolated using inverse distance weighting to the 30 m model grid. There were approximately 600,000 computational elements (pixels) for each of which independent water and energy balance solutions were found using spatially distributed forcing data, soils, land cover and soils-topographic index.

2.3. Model results

2.3.1. Washita '92

The conditions leading up to the June 1992 experiment were wet, including a rainfall event on June 9, followed by a steady dry-down until the end of the experiment on June 18. As discussed in [11], the airborne ESTAR was flown daily during Washita '92, and the derived soil moisture products have been validated against gravimetric measurements on a field-by-field basis. These products are used in the current work for comparison with the model-predicted 5 cm volumetric soil moisture. Fig. 2 shows ESTAR and model-predicted soil moisture for June 18. It is important to note that the pattern is well represented by the model, including the dry-down of the bare soil (formerly winter wheat) fields to the west as well as the signature of the wetter areas around the stream to the east. As discussed in the introduction, the ESTAR images from June 11, 14 and 18 have been analyzed by Rodriguez-Iturbe et al. [23] and others, and the model-derived images from the entire simulation will be analyzed in the scaling analysis described later. Fig. 3 shows a scatter plot of model-predicted soil moisture for each field site. While there is a tendency for the model to be slightly wet, the model is generally within one standard deviation of the field measurements. Overall, these results indicate that the model reasonably represents the spatial pattern of soil moisture in Washita '92.

2.3.2. Washita '94

The conditions leading up to the August 1994 experiment were quite dry, until a strong mesoscale convective system (MCS) passed through the area on August 18 leaving generally wet conditions. A small event occurred overnight and in the morning on August 20, and the rest of the experiment was dry. The total precipitation for the period August 18–22 was 21.4 mm, of which 13.7 mm was evaporated (based on our model

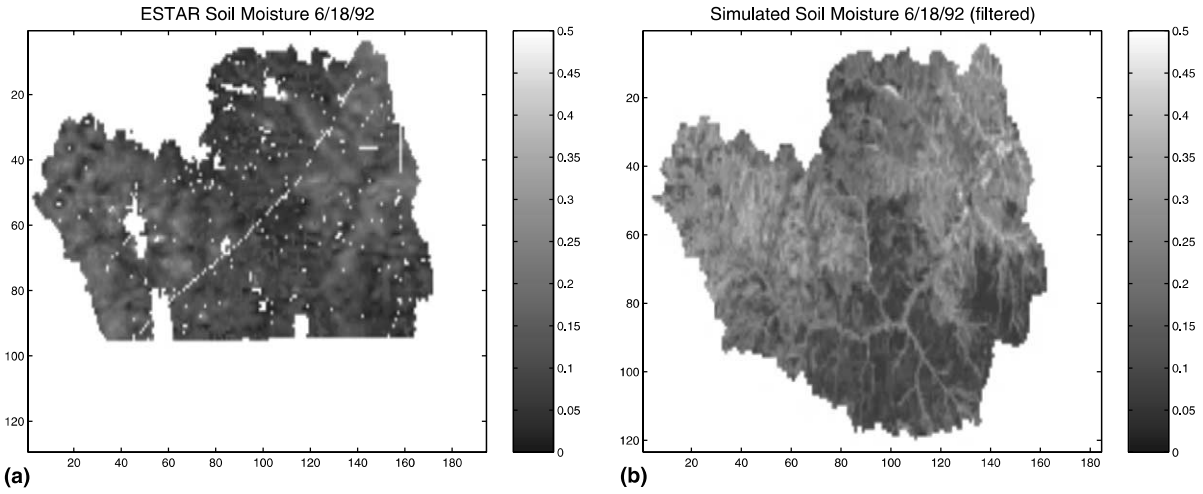

Fig. 2. Images of ESTAR (a) and model-derived (b) 5 cm soil moisture for June 18, 1992. ESTAR resolution is 200 m, and original model resolution is 30 m. Model image has been averaged to 210 m to yield spatial resolution comparable to the ESTAR. White spots in the ESTAR image represent missing data.

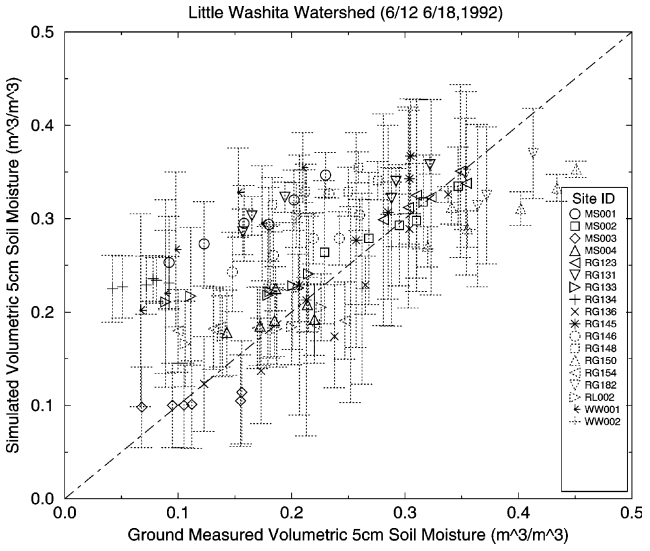

Fig. 3. Scatter plot of field-scale gravimetric versus modeled 5 cm soil moisture for period June 12–18, 1992. The error bars represent the standard deviation of simulated soil moisture, as each field is about 1 km × 1 km and consists of over 100 model grids.

calculations). The measured stream flow at the outlet of the watershed was generally less than 10 cfs, with a total of 0.5 mm for the experimental period. Due to the low flows at this time, most of the USGS stream flow values were estimated, and therefore, the stream flow was not particularly useful or of primary importance in validating the water balance.

In subsequent analyses, we will define the "wet" day of the experiment to be August 18 (day 230) 1994 and the "dry" day to be August 22 (day 234). An analysis of the spatial statistics and distributions of the model predictions for these dates (see [17] for details) indicates that the latent heat flux, soil moisture and sensible heat flux have the highest CVs for the experiment. Also, the distribution of water table depth remains nearly constant and is highly negatively skewed. The skewness of the soil moisture changes dramatically between the wet and dry days, indicating that the representation of the moisture in mesoscale models by one "effective" value on the dry day is probably not appropriate [15].

The evapotranspiration is the largest component of the water balance next to precipitation. Latent and sensible heat flux were measured half-hourly at three sites across the watershed using eddy correlation systems as described in [25]. In addition, the net radiation, ground heat flux, soil temperature and other micrometeorological variables were measured at these sites. Figs. 4 and 5 illustrate a comparison with pasture and

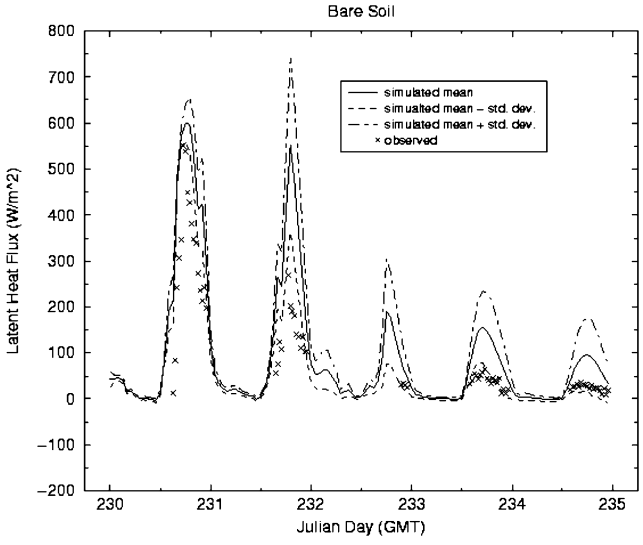

Fig. 4. Modeled and measured energy balance time series for bare soil flux station during the August Washita '94 field program.

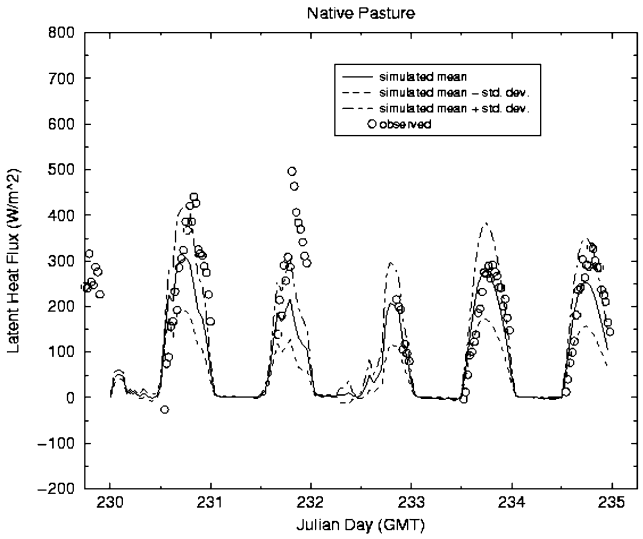

Fig. 5. Same as Fig. 4 but for native pasture.

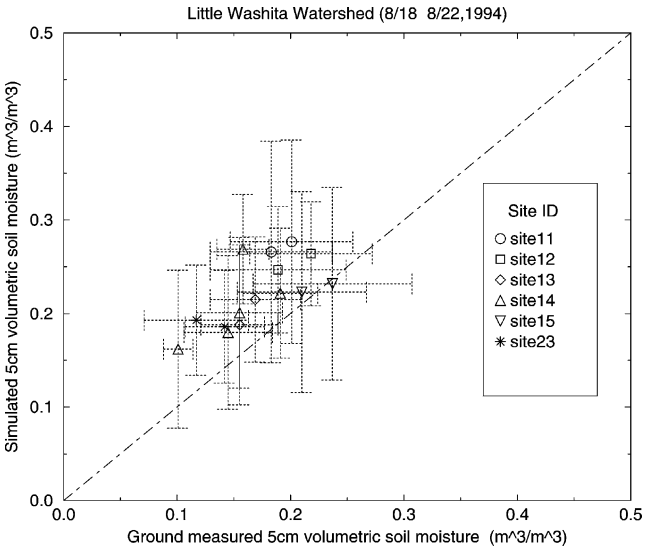

Fig. 6. Modeled and gravimetric 5 cm volumetric soil moisture for the August Washita '94 field program. Error bars indicate standard deviations for gravimetric and modeled fields. Site IDs indicate each field where gravimetric sampling was conducted as described by Starks and Humes [25].

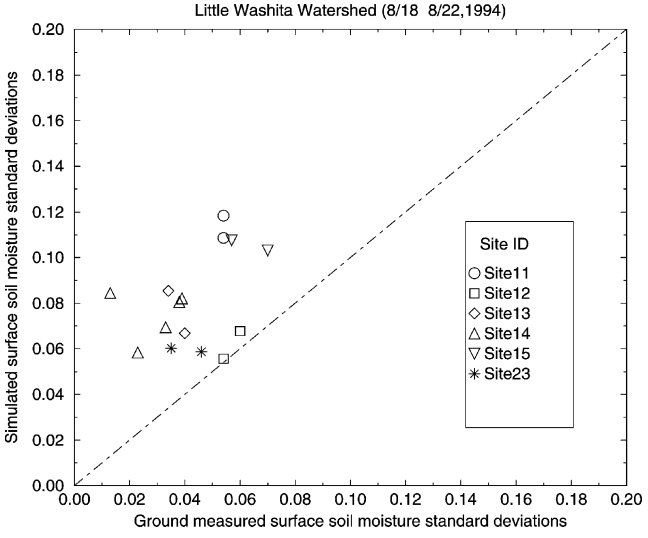

Fig. 7. Modeled and gravimetric 5 cm volumetric soil moisture spatial standard deviations for the August Washita '94 field program. Site IDs indicate each field where gravimetric sampling was conducted as described by Starks and Humes [25].

bare soil sites in the vicinity of the flux stations. These values indicate good agreement within the range of errors in the data and the spatial variability predicted by the model (to be discussed). For example, the manufacturer of the net radiometers discovered a calibration problem which led to underestimates of about 17–20% on the net radiation for certain times [Prueger J, pers. comm., 1995]. Note also that all parameters were estimated without attempting to calibrate the model.

Gravimetric soil moisture samples were taken at flux and sounding sites (four fields) for all days of the experiment, while "full" sampling (10 fields) was conducted only during the NASA/JPL airborne synthetic aperture radar (AIRSAR) overpasses (August 19 and 20). The AIRSAR soil moisture product is not available. Field averages and standard deviations of volumetric soil moisture derived from these data and collocated bulk density measurements are shown in Fig. 6 along with field averages and standard deviations of model-predicted 5 cm soil moisture. This figure indicates reasonable agreement, with some tendency for the modeled mean to be wet but within the standard deviation of the measurements. Fig. 7 shows the field versus modeled standard deviations (shown as error bars in Fig. 6) separately in order to evaluate the model's ability to simulate the spatial variability of soil moisture. As shown in the figure, the model tends to yield more variability than the observations, which are based on approximately 15 samples per field. This is not unexpected, since 15 samples is not necessarily sufficient to characterize the variability of soil moisture at the field scale. As in Washita '92, the model seems to do a reasonable job of predicting soil moisture in Washita '94 given the limited amount of validation data available.

Based on our analyses of modeled versus measured 5 cm volumetric soil moisture and latent heat flux, we can now with reasonable confidence analyze the spatial structure of modeled soil moisture and latent heat flux. The analysis that follows will focus on the Washita '94 results, although the Washita '92 results are similar.

Fig. 8 shows the spatial CV of 5 cm and "lower zone" soil moisture. The lower zone is basically an unsaturated transmission zone between the 5 cm layer and the water table. It may contain vegetation roots and it may be of variable depth, depending on the depth of the water table. This figure shows that there is a very slight trend

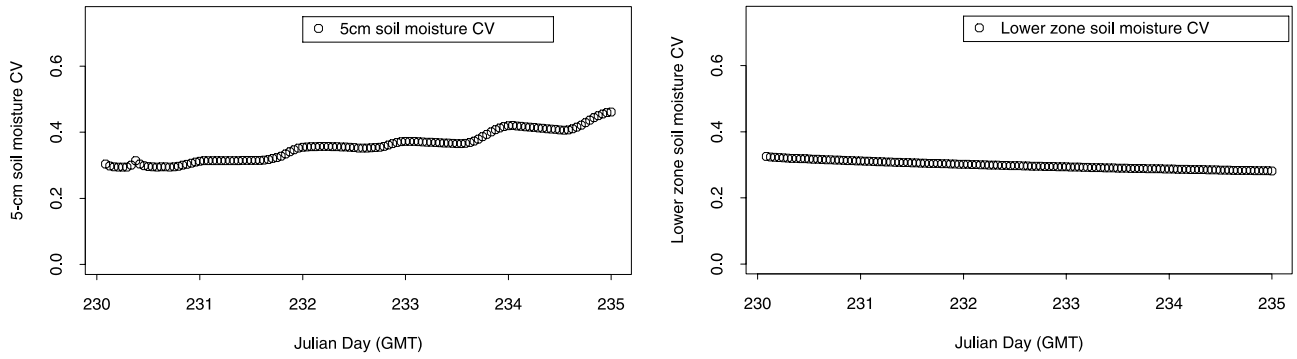

Fig. 8. Modeled spatial CV time series for 5 cm and lower zone soil moistures during the August Washita '94 field program.

towards increasing CV as the soil moisture decreases. In contrast, the lower zone CV shows a slight decrease. In general, they are quite constant throughout the experiment.

Fig. 9 shows the spatial CV for all four components of the energy balance, and each is plotted at the same scale. Immediately, we notice that net radiation has almost no variation, except for part of day 231 (August 19; partly cloudy) and day 232 (August 20; cloudy, rain). The CV of latent heat flux shows a positive trend on days 230 and 231 (August 18 and 19), and again on days 233 and 234 (August 21 and 22). However, the CV remains less than 1.0 for the experiment, and the trend is due mostly to the decreasing magnitude of the latent heat flux. The sensible heat flux, by contrast, yields very high values (>1.5) following the rainfall (again due mostly to low sensible heat values), and continues to decrease as the watershed dries out. Although all sensible heat values less than 25 W m^{-2} were filtered from this data, there is a trend toward increasing CVs at the end of each day. The ground heat flux CVs are quite small and show little trend during the experiment, except on day 232 (August 20) after the rainfall occurred. This is most likely due to spatial variability in cloudiness, since we see a nearly identical trend in the net radiation.

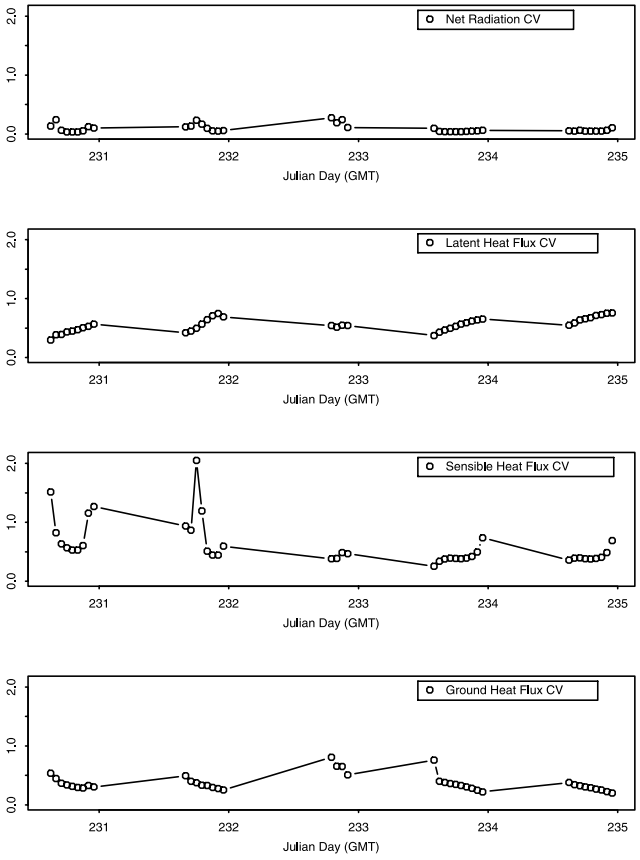

Fig. 9. Modeled spatial CV time series for components of the energy balance during the August Washita '94 field program.

3. Scaling characteristics of hydrologic variables

3.1. Review of notation

In this section, we perform a scaling analysis of model-predicted 5 cm soil moisture in the manner of [4,9]. These works and the references therein present an excellent overview of literature related to scaling theory and scaling analyses of hydrologic variables. Therefore, the reader is referred to these references for additional information. In addition, the notation is identical to that of [4], and presented here for clarity.

Consider an image with dimensions 256×256. If we average the pixel values to obtain one value over the entire image, we define the scale factor for the resulting 1×1 image as $\lambda = 1$. If we then start dividing the image such that the dimensions of the finer images are two times that of the coarser image, we obtain scale factors which are inverse powers of two: $\lambda = 1/2^1,\ 1/2^2,\ 1/2^3, \ldots = 1/2,\ 1/4,\ 1/8, \ldots$ Thus, for a 256×256 image, the finest scale factor is $\lambda = 1/2^8 = 1/256$. We will define $\lambda = 1$ as a reference value corresponding to the coarsest aggregation considered; thus $\lambda \leqslant 1$ since it is simply the ratio of a given resolution to that of the coarsest resolution. These definitions are consistent with those of [8].

A process ϕ is defined as spatially scaling with respect to moment q if the following relationship holds:

$$E[(\phi_\lambda)^q] \propto \lambda^{K(q)} E[(\phi_1)^q], \tag{3}$$

where $K(q)$ is the scaling exponent associated with moment q. For a "simple scaling" process, the exponents $K(q)$ are linear in q:

$$K(q) = Cq, \tag{4}$$

where the coefficient C is a constant. Such a process may be termed "fractal" or "monofractal". If $K(q)$ is nonlinear, then the process is said to be multiscaling. Typically, multiscaling fields exhibit a convex (downward, given our definition of λ) $K(q)$, as in [8,22]. It is important to note that we give λ to the $K(q)$ in Eq. (3),

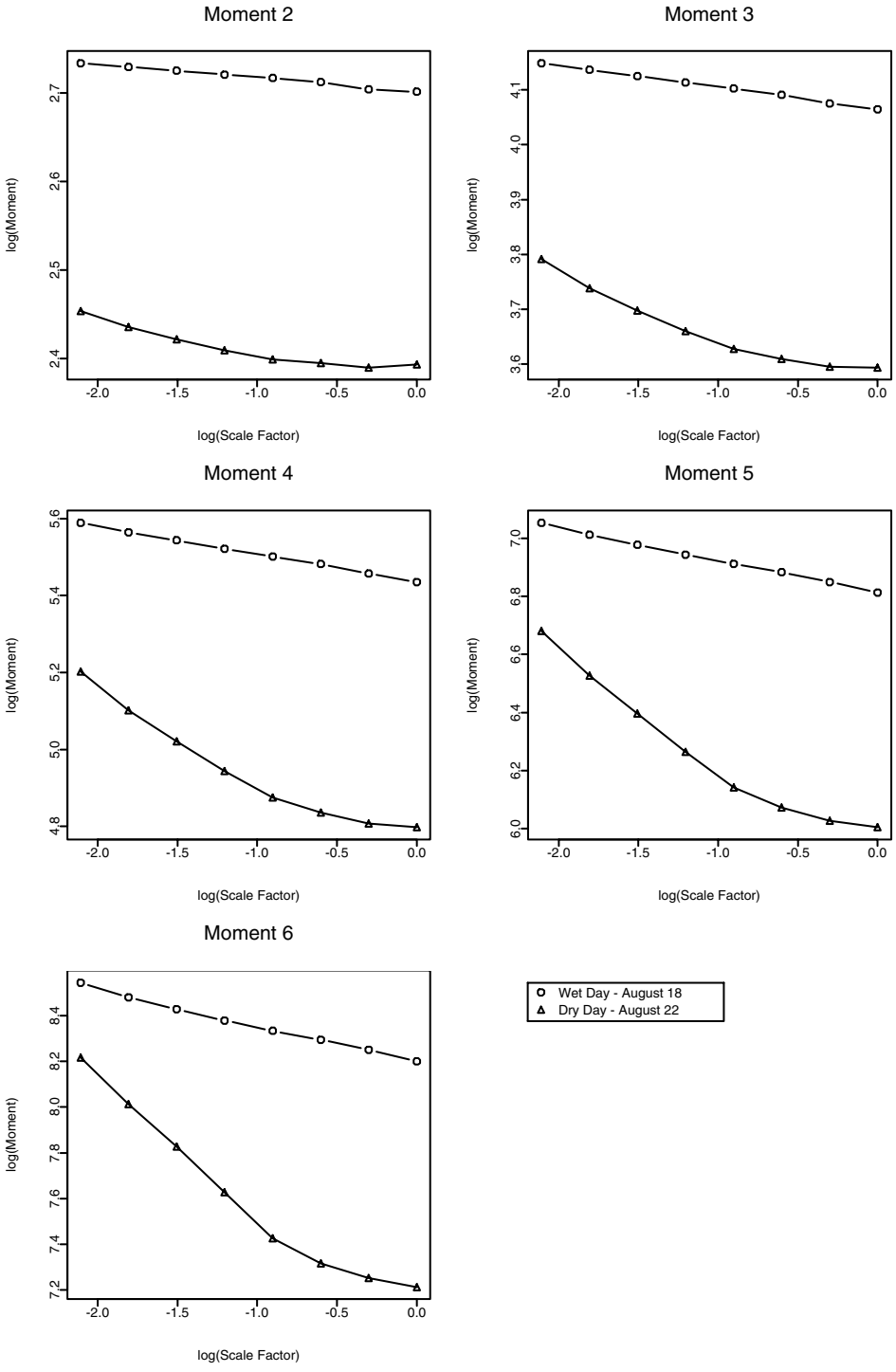

Fig. 10. Scaling behavior of second through sixth moments of solar noon 5 cm soil moisture on "wet" and "dry" days of Washita '94.

rather than λ^2 to the $K(q)$ as in [9]; therefore our $K(q)$ will differ by a factor of 2 as compared to those of [9].

Eq. (3) can be a very powerful tool for modeling subgrid scale processes in coarse-resolution models, because it implies that statistical properties of model fields may be determined if we can estimate its scaling exponents a priori. By definition, scaling exponents are not a function of scale; therefore if we can estimate them at a coarse scale, we can infer statistics at a fine scale.

3.2. Model-predicted soil moisture

Fig. 10 shows the results of an empirical evaluation of the moments of modeled Washita '94 5 cm volumetric soil moisture ($\phi = \theta$) versus scale factor λ, as defined above. The largest scale factor had an aggregation size of 128×128 (3840 m). The graphs show what appears to be simple scaling behavior for the wet day and multiscaling behavior for the dry day.

The results of an unweighted least-squares regression on the values shown in Fig. 9 were used to estimate the scaling exponent $K(q)$ of (3). In general the fits were better for the wet day than the dry day for Washita '94. On the dry day, the most linear portion of the graph was used in the fit, so as to maximize the coefficient of determination.

The scaling exponents are plotted against the q in Fig. 11 for Washita '94 which, along with Fig. 10, suggests that modeled 5 cm soil moisture shows signs of multiscaling for the dry day, in particular. The first moment, which was not shown on Fig. 10, is shown here simply to confirm that our algorithm was working properly, since the mean of the field should not change, unless the averaging area is changing due to the exclusion of pixels (near the edge, for example).

Fig. 12 illustrates the full transition from "wet" to "dry" during Washita '92 as predicted by the model. This behavior is consistent with that of remotely sensed soil moisture products in the Little Washita Watershed analyzed in [4,9,23] for the same period, although the focus of the prior work has been on the days June 11, 14 and 18. Unfortunately, no remotely sensed soil moisture products exist for the August campaign of Washita '94 analyzed here. Therefore, in order to further investigate the "observed" scaling behavior as a function of

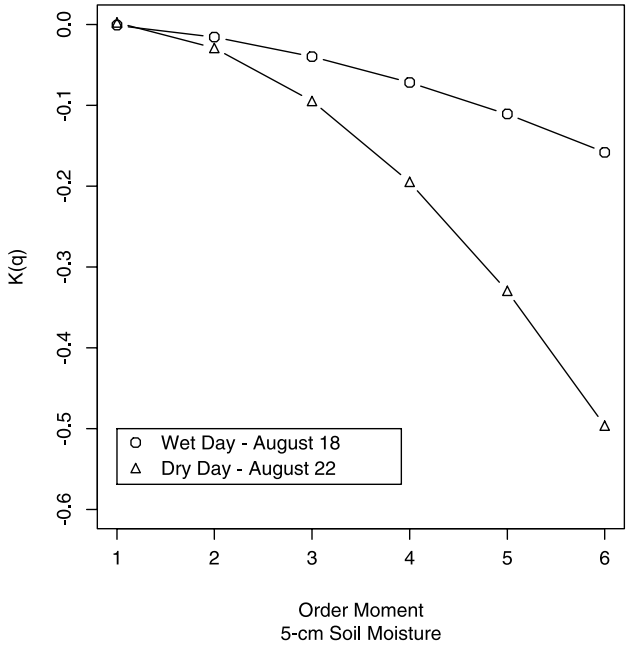

Fig. 11. Scaling exponent versus order moment for solar noon 5 cm soil moisture on "wet" and "dry" days. Multiscaling behavior is exhibited on the dry day.

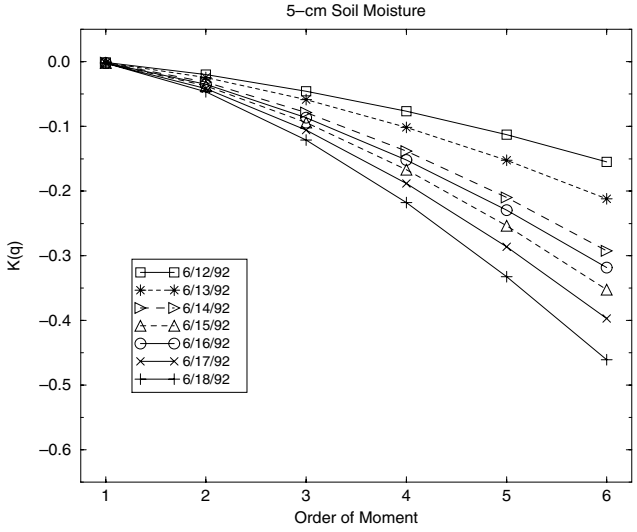

Fig. 12. Model-derived scaling exponent versus order moment for solar noon 5 cm soil moisture for Washita '92.

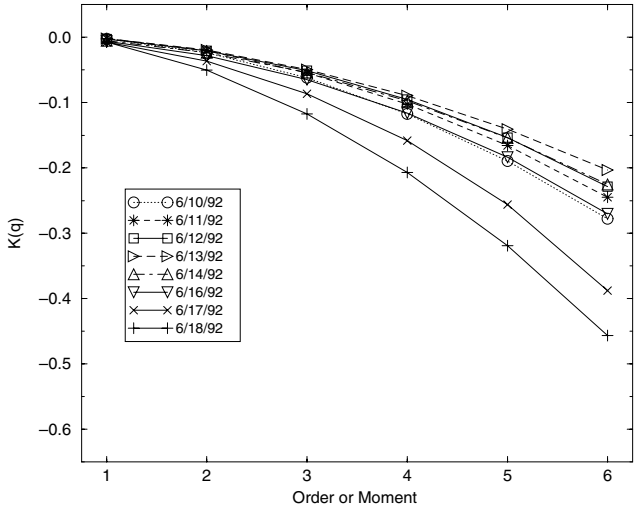

Fig. 13. Scaling exponent versus order moment for ESTAR-derived soil moisture from Washita '92.

moisture content, we re-analyze the ESTAR data from Washita '92 in the next section.

3.3. Observed soil moisture

Fig. 13 illustrates the observed multiscaling characteristics derived as described in the previous section. From this figure, we find that non-linearity of the slope as a function of q (order of moment) increases during dry-down, with prior analysis of the 1992 data as well as the modeling results discussed above.

These results suggest some important observations. First, the models discussed in [4,27] did not reproduce the observed scaling behavior with time, as noted by

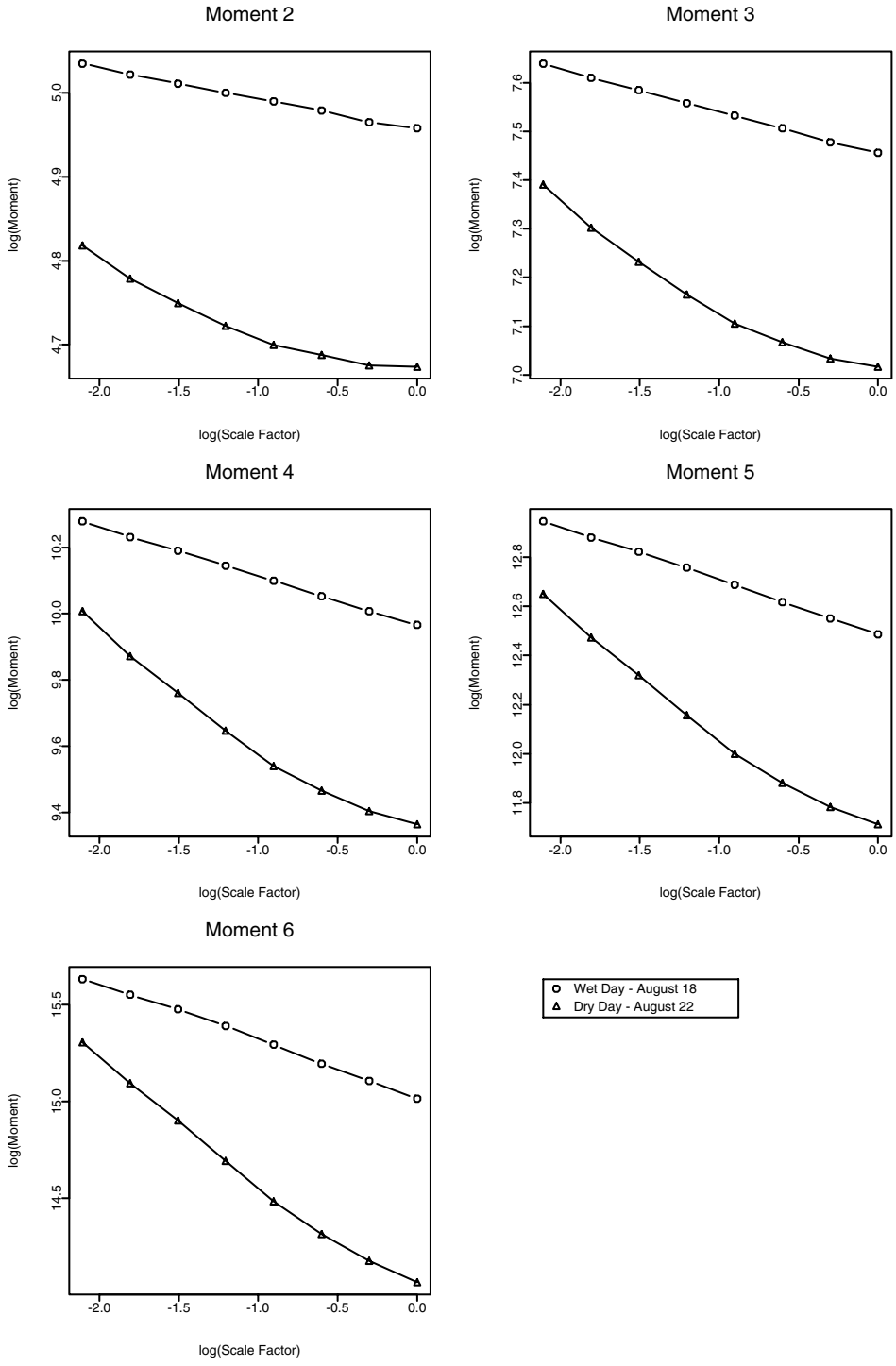

Fig. 14. Scaling behavior of second through sixth moments of solar noon latent heat flux on "wet" and "dry" days.

Dubayah et al. [4] and Hu et al. [9]. Second, as noted above, the model used in this work differs fundamentally from the others in that it *explicitly* represents the spatial distributions of soil properties as well as vegetation. Presumably, this leads to the improved representation of soil moisture scaling properties during the dry-down. Further evidence for this is suggested by comparing Fig. 1 in [4] with Fig. 2 above. In Fig. 1(a) of [4], one notes the relatively "dry" regions west of the large missing data portion. We suspect that these were bare soil areas (formerly winter wheat fields) in 1992, similar to those evident in Fig. 2 for the "dry" day in 1994. In contrast, Fig. 1(b) from [4] looks quite similar to Fig. 2, except that the flood plain and stream channel are less well defined. This is due to a revised topographic index map used in this work.

In the following section, we perform an identical scaling analysis on model-predicted latent heat flux, which is of critical importance for land–atmosphere interaction modeling.

3.4. Model-predicted latent heat flux

Figs. 14 and 15 are similar to Figs. 10 and 11, except for modeled latent heat flux. The figures clearly suggest multiscaling behavior which becomes more marked for the dry day. It is interesting to note that the soil moisture results indicate more non-linearity in the scaling exponents with respect to order moment than do the latent heat flux results. In addition, the magnitudes of the scaling exponents are similar, with the latent heat flux exponents consistently less (greater absolute value) than the soil moisture exponents.

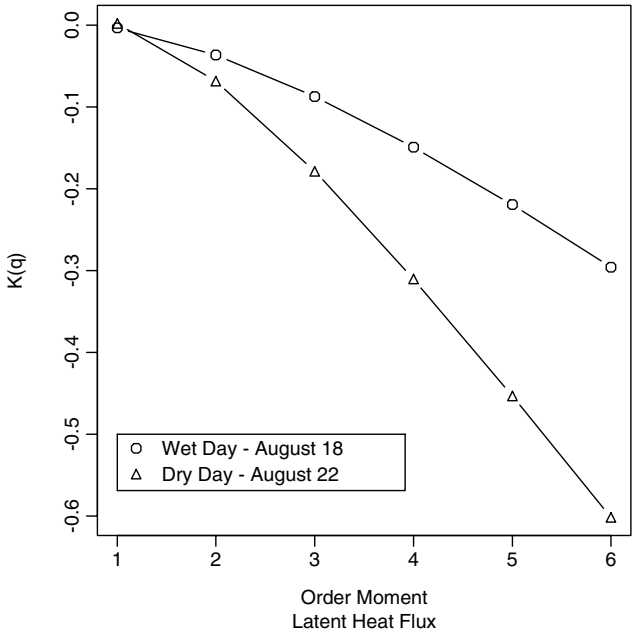

Fig. 15. Scaling exponent versus order moment for solar noon latent heat flux on "wet" and "dry" days. Multiscaling behavior is exhibited on the dry day.

4. Implications for land surface modeling

Currently, most land surface models utilize "effective" values of soil moisture to predict latent heat flux at the grid scale. As shown by Li and Avissar [15], a highly skewed subgrid distribution of soil moisture will not produce the equivalent grid-averaged latent heat flux to that produced the mean soil moisture. Therefore, it might be necessary to employ or derive probability distribution functions of subgrid soil moisture in order to predict the proper grid-averaged latent heat flux. Given that both latent heat flux and soil moisture seem to exhibit multiscaling behavior, which changes with moisture condition, it is desirable to investigate the existence of a simple (e.g. quadratic) relationship between $K(q)$ and q which is also a function of moisture condition.

4.1. Multiscaling regimes

For Washita '92, Figs. 12 and 13 suggest a nearly monotonic behavior of $K(q)$ vs. q during dry-down. However, past work on the subject (discussed above) has focused primarily on three days during the experiment: June 11, 14 and 18. Although these days exhibit a monotonic behavior of their scaling exponents with dry-down, Fig. 16 shows that the behavior of ESTAR-derived scaling exponents is not monotonically decreasing. In fact, there seem to be three distinct regimes, from June 10 to 13, June 13 to 16, and June 16 to 18. One might hypothesize that these regimes correspond to transitions from "atmospheric/infiltration-dominated"

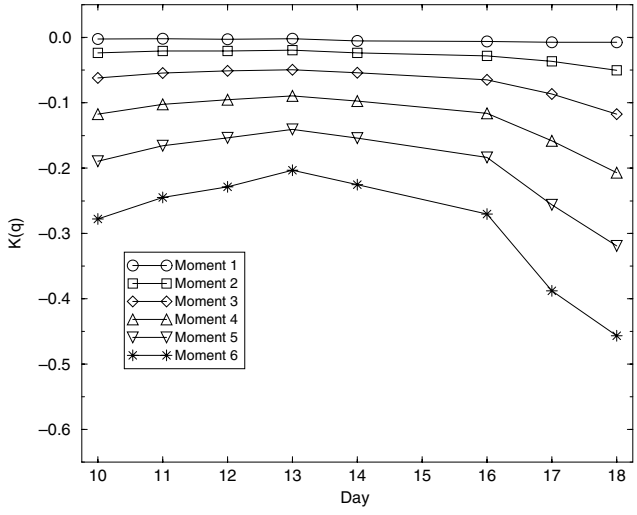

Fig. 16. Time series of scaling exponents for ESTAR soil moisture.

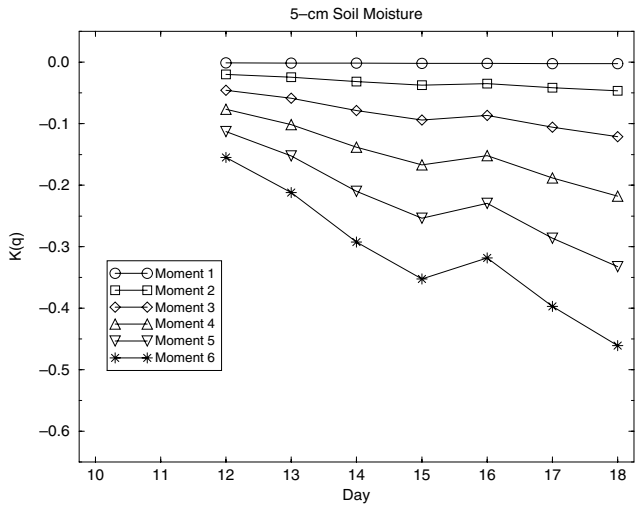

Fig. 17. Time series of scaling exponents for modeled 5 cm soil moisture.

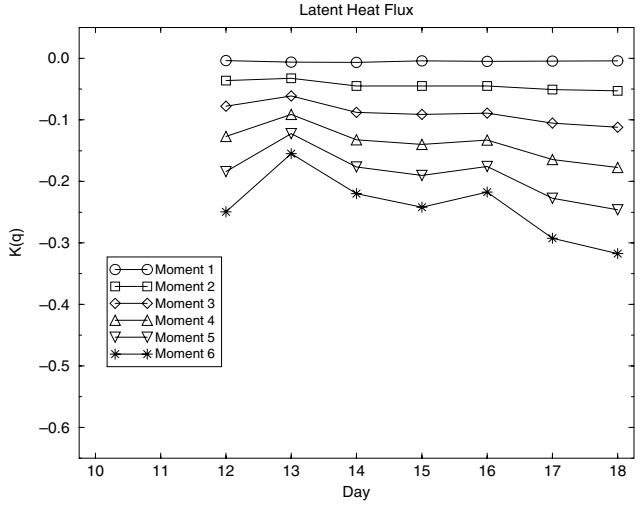

Fig. 18. Time series of scaling exponents for modeled latent heat flux.

(regime 1) to "transitional" (regime 2) to "drainage/evaporation-dominated" (regime 3) control during the interstorm period.

Figs. 17 and 18 illustrate the behavior of model-predicted moments versus time. Both figures seem to indicate the representation of the second and third regime by the model, although the first regime is not represented. A probable cause for this is the fact that the atmospheric forcings (and in particular, the precipitation) might not be well represented by the available data.

4.2. Simple scaling model for regimes 2 and 3

During Washita '94, the model-predicted scaling behavior is again monotonic with time. Similar to Washita '92, this behavior is most likely associated with transitions from infiltration (regime 2) to drainage/evaporation (regime 3). We illustrate this behavior in a slightly different plot as compared to Figs. 16–18.

Fig. 19 shows a perspective plot of $Z = K(q)$ versus $X =$ order moment (q) versus $Y =$ spatial average soil moisture $(\bar{\theta})$ in percent for scaling exponents of both 5 cm soil moisture and latent heat flux. The lines shown in Figs. 11 and 15 form the two ends of the surfaces. This figure suggests the existence of a smoothly varying function $K(q, \bar{\theta})$ (for soil moisture in particular), which might be applicable in regimes 2 and 3.

An interesting feature of Fig. 19, which was not evident in Fig. 15, is the "kink" which occurs near the middle of the surface. This has been found to be the days of the experiment August 19 and 20, which were partly cloudy, with some rain (as discussed above). Therefore, it is a reasonable hypothesis that the spatial scaling properties of latent heat flux would be strongly affected by the radiative properties (e.g. cloud cover) in addition to soil moisture. This hypothesis was not tested in the present work, and is presented merely as an interpretation. Finding a potential scaling model for latent heat flux could be potentially as useful as one for soil moisture in the context of land surface modeling, and is the subject of ongoing work. However, for subsequent analysis in this work, we propose a relationship of the form for both soil moisture and latent heat flux (where missing cross-terms were dropped due to lack of statistical significance):

$$K(q,\bar{\theta}) = a + bq + cq^2 + d\bar{\theta} + e\bar{\theta}^2 + fq\bar{\theta} + gq^2\bar{\theta} + hq\bar{\theta}^2 + iq^2\bar{\theta}^2. \quad (5)$$

The best fit to this relationship is given by the following for soil moisture (with $\bar{\theta}$ in percent):

$$K(q,\bar{\theta}) = -0.12 - 0.60q - 0.14q^2 + 0.23\bar{\theta} + 1.19q\bar{\theta} + 0.33q^2\bar{\theta}, \quad (6)$$

where all terms shown are accepted at the 0.01 confidence level. Terms not shown were not found to be significant at this level. The following expression gives the best fit for latent heat flux scaling exponents:

$$K(q,\bar{\theta}) = -0.18 - 0.75q - 0.075q^2 + 0.24\bar{\theta} + q\bar{\theta}, \quad (7)$$

where as before $\bar{\theta}$ is expressed in percent, and the all terms not shown are rejected at the 0.01 confidence level. Fig. 20 shows a plot of the fitted relationships, which can be compared to Fig. 19. Given that both soil moisture and latent heat flux appear to be multiscaling, it is desirable that future investigations of this type search for general relationships as a function of readily available parameters such as porosity.

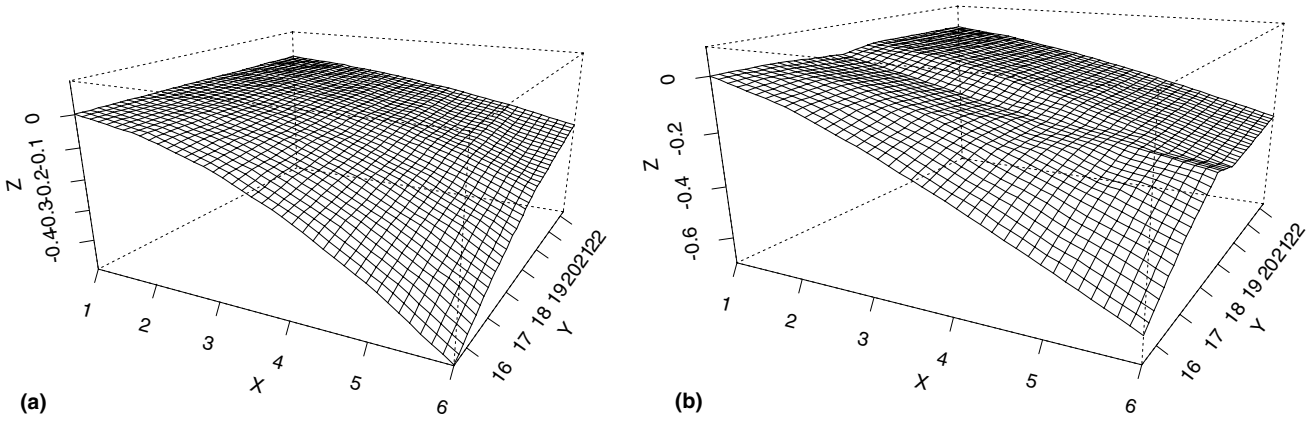

Fig. 19. Empirical $K(q,\bar{\theta})$ relationships for (a) soil moisture and (b) latent heat flux. $X =$ order moment, $Y =$ soil moisture (%), $Z = K(q,\bar{\theta})$.

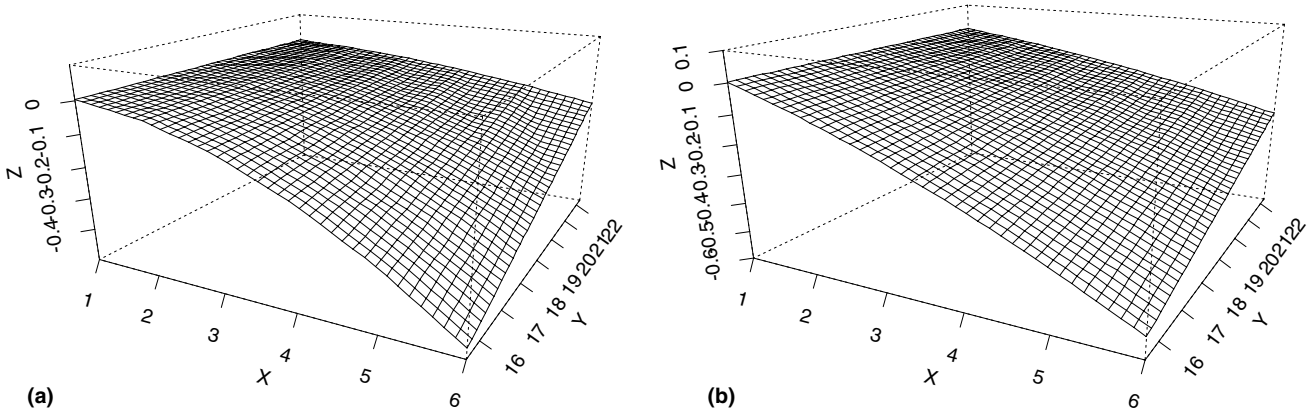

Fig. 20. Fitted $K(q,\bar{\theta})$ relationships for (a) soil moisture and (b) latent heat flux. $X =$ order moment, $Y =$ soil moisture (%), $Z = K(q,\bar{\theta})$.

4.3. Physical controls on soil moisture multiscaling

Finally, we revisit the land surface parameters which presumably lead to this multiscaling behavior. Fig. 21 illustrates the physical soil moisture "end points" of field capacity and wilting point and/or residual soil moisture, as well as the other factors in land surface modeling including soils-topographic index, porosity and leaf area index. These parameters are the dominant controls on infiltration, drainage and evaporation of water from soils, and as indicated by Fig. 21, the field capacity exhibits simple scaling, while the residual moisture content suggests multiscaling. The field capacity behavior is consistent with that observed by Rodriguez-Iturbe et al. [23] for porosity.

This figure indicates simple scaling for porosity, field capacity and wilting point, and multiscaling for residual soil moisture, leaf area index and the soils-topographic index. If one thinks of porosity, field capacity and leaf area index (via interception) as controlling infiltration, and soils-topographic index (via its effect on water table depth), leaf area index (via transpiration), wilting point and residual moisture content as

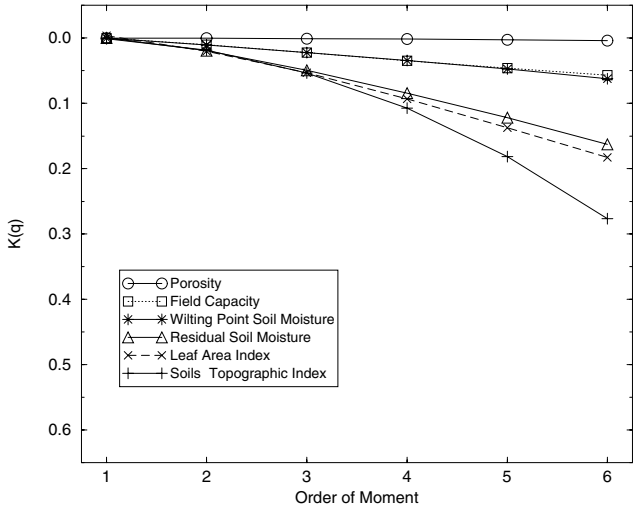

Fig. 21. Scaling exponent versus order moment for land surface parameters.

controlling drainage and evaporation, then it seems plausible that the increased non-linearity in the soil moisture scaling exponents during dry-down is due

primarily to a shift from infiltration-controlled to drainage- and/or evaporation-controlled. These should directly correspond to the regimes 1–3 shown above, although this hypothesis must be tested with more data and modeling studies.

One serious caveat to the above results is that the scaling properties of both the model-predicted fluxes and states as well as the land surface parameters been affected by the inherent resolution of the forcing data as well as the original topographic, soil and land cover datasets from which they were derived. We have attempted to use the finest spatial resolution data available for this type of analysis, and we fully expect that resolutions will continue to improve with time.

5. Conclusions

We have investigated the spatial structure of 5 cm soil moisture and surface latent heat fluxes for the June Washita '92 field experiment and the August campaign of the Washita '94 field experiment using a spatially distributed water and energy balance model. The model has been shown to reasonably represent soil moisture and latent heat flux during both experimental periods. Analyses of the statistics of the modeled fluxes and states indicate significant changes in those statistics with moisture condition, and the largest spatial variability is seen in latent and sensible heat flux and 5 cm soil moisture.

Scaling analysis of model-predicted soil moisture from both experimental periods is indicative of multiscaling behavior, which increases with dry-down, consistent with previous analyses of the Washita '92 data. This is the first time, to our knowledge, that a model has been shown capable of representing time-varying scaling properties of soil moisture. Another new result of this work is that modeled latent heat flux also exhibits multiscaling behavior, and that this behavior appears to be explained to first order by the scaling properties of modeled moisture availability. The full representation of this relationship was not determined, but is believed to be a convolution of soil moisture with the radiative forcings as well as vegetation. The multiscaling behavior of soil moisture is hypothesized as a relationship which is a function of average soil moisture, which seems to fit the data quite well.

The temporal behavior of the scaling exponents for various moments derived from ESTAR for Washita '92 suggests the existence of three distinct regimes during a dry-down. This is consistent with model results, which indicate a transition from simple scaling to multiscaling with dry-down. It is hypothesized that this transition is governed by the scaling properties which control infiltration (porosity, field capacity, leaf area index, in the case of wet conditions) to properties which control drainage (residual moisture content, soils-topographic index) and evaporation (wilting point, leaf area index).

More work is needed to further investigate the mechanistic causes for the multiscaling of soil moisture and latent heat flux fields in order to enable prediction of higher-order moments from coarse-resolution data. Preliminary results from a related study for the Southern Great Plains 1997 Hydrology Experiment (SGP97) [10] indicate similar multiscaling behavior of soil moisture during dry-down, and this work will be the subject of a future publication.

Acknowledgements

The authors thank Bill Kustas for providing the meteorological and flux data for Washita '92, and John Prueger for providing the flux data for Washita '94. We also thank Ralph Dubayah for providing an early version of code to compute moments for various scale factors. This material is based on work supported by a National Science Foundation Graduate Research Fellowship and a George Van Ness Lothrop Fellowship in Engineering from The Graduate School at Princeton University. Additional support from the following is gratefully acknowledged: NASA contract NAS5-31719 entitled "Global hydrological processes and climate" (Wood); NOAA grant NA56GP0249 entitled "Development and testing of a macroscale hydrologic model for the southern plains region of GCIP" (Wood); and NASA grant NAG5-8698 entitled "Quantifying the relationship between remotely sensed and modeled soil moisture" (Peters-Lidard).

References

[1] Beven KJ, Kirkby MJ. A physically based, variable contributing area model of basin hydrology. Hydrol Sci Bull 1979;24(1):43–69.

[2] Brutsaert W. Evaporation into the atmosphere: theory, history, and applications. Dordrecht: Kluwer Academic Publishers; 1982 [299 p.].

[3] Burrough PA. Multiscale sources of spatial variation in soil: the application of fractal concepts to nested levels of soil variation. J Soil Sci 1983;34:577–91.

[4] Dubayah R, Wood EF, Lavalée D. Multiscaling analysis in distributed modeling and remote sensing: an application using soil moisture. In: Goodchild MF, Quattrochi DA, editors. Scales in remote sensing and GIS. Boca Raton (FL): CRS/Lewis Publishers; 1997. p. 93–111.

[5] Famiglietti JS, Wood EF. Application of multiscale water and energy balance models on a tallgrass prairie. Water Resour Res 1994;30(11):3061–78.

[6] Famiglietti JS, Wood EF. Effects of spatial variability and scale on areally averaged evapotranspiration. Water Resour Res 1995;31:699–712.

[7] Grayson RB, Western AW, Chiew FHS, Bloschl G. Preferred states in spatial soil moisture patterns: local and nonlocal controls. Water Resour Res 1997;33(12):2897–908.

[8] Gupta VK, Waymire EC. Multiscaling properties of spatial rainfall and river flow distributions. J Geophys Res 1990;95:1999–2009.
[9] Hu Z, Chen Y, Islam S. Mutiscaling properties of soil moisture images and decomposition of large- and small-scale features using wavelet transforms. Int J Remote Sensing 1998;19(13):2451–67.
[10] Jackson TJ. Southern Great Plains 1997 (SGP97) Experiment plan. 1996. Available from: http://hydrolab.arsusda.gov/sgp97/.
[11] Jackson TJ, Le Vine DE. Mapping surface soil moisture using an aircraft-based passive microwave instrument: algorithm and example. J Hydrol 1996;184:85–99.
[12] Jackson TJ, Schiebe FR, editors. Hydrology data report: WASH-ITA '92. NAWQL-93-1, National Agricultural Water Quality Laboratory, USDA Agricultural Research Service, Durant (OK), 1993.
[13] Jacquemin B, Noilhan J. Sensitivity study and validation of a land surface parameterization using the HAPEX-MOBILHY data set. Boundary-Layer Meteorol 1990;52:93–134.
[14] Kustas WP, Stannard DI, Allwine KJ. Variability in surface energy flux partitioning during Washita '92: resulting effects on Penman–Monteith and Priestly–Taylor parameters. J Agric For Meteorol 1996;82:171–93.
[15] Li B, Avissar R. The impact of spatial variability of land-surface characteristics on land-surface heat fluxes. J Climatol 1994;7:528–37.
[16] O'Neill P, Hsu A, Jackson T, Wood E, Zion M. Investigation of the accuracy of soil moisture inversion using microwave data and its impact on watershed hydrological modeling. In: Proceedings of the Third International Workshop on Application of Remote Sensing in Hydrology, NHRI Symposium Series, 1996 October 16–18; Greenbelt, MD, 1996. p. 211–26.
[17] Peters-Lidard CD. The effect of land surface heterogeneity on land–atmosphere interactions. Ph.D. Dissertation, Department of Civil Engineering and Operations Research, Princeton University, 1997.
[18] Peters-Lidard CD, Blackburn E, Liang X, Wood EF. The effect of soil thermal conductivity parameterization on surface energy fluxes and temperatures. J Atmos Sci 1998;55(7):1209–24.
[19] Peters-Lidard CD, Zion MS, Wood EF. A soil–vegetation–atmosphere transfer scheme for modeling spatially variable water and energy balance processes. J Geophys Res 1997;102(D4):4303–24.
[20] Pielke RA. Mesoscale meteorological modeling. Orlando: Academic Press; 1984 [612 p.].
[21] Rawls WJ, Brakensiek DL, Saxton KE. Estimation of soil water properties. Trans Am Soc Agric Eng 1982;25:1316–20.
[22] Rodriguez-Iturbe I, Marani M, Rigon R, Rinaldo A. Self-organized river basin landscapes: fractal and multifractal characteristics. Water Resour Res 1994;30(12):3531–9.
[23] Rodriguez-Iturbe I, Vogel GK, Rigon R, Entekhabi D, Castelli F, Rinaldo A. On the spatial organization of soil moisture fields. Geophys Res Lett 1995;22:2757–60.
[24] Sivapalan M, Beven K, Wood EF. On hydrologic similarity, 2. A scaled model of storm runoff production. Water Resour Res 1987;23(12):2266–78.
[25] Starks PJ, Humes KS, editors. Hydrology data report: WASH-ITA '94. NAWQL-96-1, National Agricultural Water Quality Laboratory, USDA Agricultural Research Service, Durant (OK), 1996.
[26] Western AW, Grayson RB, Bloschl G, Willgoose G, McMahon TA. Observed spatial organisation of soil moisture and relation to terrain indices. Water Resour Res 1999;35(3):797–810.
[27] Wood EF. Scaling, soil moisture and evapotranspiration in runoff models. Adv Water Resour 1994;17:25–34.
[28] Wood EF. Scaling behavior of hydrological fluxes and variables: empirical studies using a hydrological model and remote sensing data. In: Kalma JD, Sivapalan M, editors. Scale issues in hydrological modeling. New York: Wiley; 1995. p. 89–104.
[29] Wood EF. Effect of soil moisture aggregation on surface evaporative fluxes. J Hydrol 1997;190:397–412.
[30] Wood EF. Scale analyses for land-surface hydrology. In: Sposito G, editor. Scale dependence and scale invariance in hydrology. Cambridge: Cambridge University Press; 1998. p. 1–29.
[31] Wood EF, Sivapalan M, Beven K. Similarity and scale in catchment storm response. Rev Geophys 1990;28(1):1–18.